INFLUENCE OF LANTHANUM SUBSTITUTION AT A-SITE ON STRUCTURAL, MORPHOLOGICAL AND ELECTRICAL PROPERTIES OF THE $La_{(0.7-x)}Ln_xCa_{0.3}MnO_3$ (LN = PR, SM, CE) NANOPARTICLES SYNTHESIZED BY PECHINI METHOD

**J. Ramírez-Hernández[1], S. B. Brachetti-Sibaja[1*],
A. M. Torres-Huerta[2*], M. A. Domínguez-Crespo[2],
M. A. Aguilar-Frutis[3], J. Moreno-Palmerín[4],
F. Gutierrez-Galicia[2]**

[1]Tecnológico Nacional de México, IT de Ciudad Madero, D.E.P.I., Ave. Primero de Mayo S.N. Col. Los Mangos, Cd. Madero, C.P. 89449, Tamps, México.

[2]Instituto Politécnico Nacional, UPII-Hidalgo, km. 1+500, Carretera Pachuca, San Agustín Tlaxiaca, Actopan, Hgo, 42162, México.

[3]Instituto Politécnico Nacional, CICATA Unidad Legaria, Calzada Legaria 694, Miguel Hidalgo, CDMX, 11500, México.

[4]Departamento de Minas, Metalurgia y Geología, Universidad de Guanajuato, Ex Hacienda San Matías s/n, Guanajuato, Guanajuato, C.P. 36020, México.

atohuer@hotmail.com, bbrachetti@hotmail.com

Ramírez-Hernández, J., Brachetti-Sibaja, S. B., Torres-Huerta, A. M., Domínguez-Crespo, M. A., Aguilar-Frutis, M. A. *et al.* (2023). Influence of lanthanum substitution at A-site on structural, morphological and electrical properties of the $La_{(0.7-x)}Ln_xCa_{0.3}MnO_3$ (Ln= Pr, Sm, Ce) nanoparticles synthesized by Pechini method. In E. San Martín-Martínez (Ed.). *Research advances in nanosciences, micro and nanotechnologies. Volume IV* (pp. 191-212). Barcelona, Spain: Omniascience.

Abstract

Solid Oxide Fuel Cells (SOFC) are one of the highly efficient energy conversion devices; however, the typical operating temperature (800 to 1000 °C) represents a challenge by requiring materials that can withstand these conditions without losing their properties. For SOFCs, the most commonly used cathode materials are lanthanum-strontium manganites (LSM); however, this type of materials has disadvantages as they require a high polarization, which has prompted the development of perovskite-type structure materials (ABO_3), establishing that combining or substituting lanthanum with some other lanthanide $(La_{1-x}Ln_x)_{0.7}Ca_{0.3}MnO_3$ could reduce the overpotential at the cathode, and increase the electrocatalytic activity. In this work, the effect of cation substitution in non-stoichiometric perovskites $(La_{1-x}Ln_x)_{0.7}Ca_{0.3}MnO_3$ (Ln=Pr, Sm, Ce) on the structural, morphological, and electrical properties has been evaluated when the Pechini method is used as a synthesis method. The properties were analyzed in terms of potential applications as cathode materials in SOFCs varying the doping concentration (x=0.1, 0.3, 0.5 and 0.6). The Pechini method is a low-cost reproducible method that led to the production of phase-pure perovskite under certain experimental conditions. The electrical conductivities at room temperature ranged between 0.5 and 0.09 S cm^{-1}, which seems promising to be used as cathode at low-intermediate temperatures preserving the activity for oxygen reduction reaction.

Keywords: Solid oxide fuel cells, nanostructures, perovskites, Pechini method.

1. Introduction

Fuel cells are a great field of study due to their development as alternative energy sources, carrying out research that proposes different synthesis methods to obtain electrode materials that provide favorable characteristics for their operation. In recent years, different works have been published that serve as a basis for the different types of cells, such is the case of Selmi *et al.* [1], where a compilation about fuel cells is provided, giving information about the challenges they currently present and the benefits they provide, making a general analysis of the different types that exist and their cost-benefit, as well as, the efficiency that they could present and their possible applications. The progress of SOFC research, the evolution of new materials, and the development of advanced instruments have collectively led to the selection of parameters that, when controlled, directly affect the desired performance results in the energy production [2].

These types of devices are normally classified according to the electrolyte used, with the exception of the direct methanol fuel cell (DMFC), where methanol is fed directly to the anode and therefore, it is the electrolyte of this cell, the second classification is based on the operating temperature of the cells. These can be classified into high and low temperature fuel cells. Low temperature fuel cells are alkaline (AFC), proton exchange cells (PEMFC), direct methanol (DMFC) and phosphoric acid fuel cells (PAFC). High temperature cells operate at temperatures from 600-1000 °C, and these are: molten carbon (MCFC) and solid oxide fuel cell (SOFC) [3]. Then, a solid oxide fuel cell is a high temperature device with a solid oxide as electrolyte which has the characteristic that it needs to be operated at an elevated temperature to achieve enough power. Knowing this, the use of cheap catalysts may be a good way to reduce the cost of the fuel cell. On the other hand, the possibility of using biofuel instead of hydrogen could be considered an eco-friendly alternative [4].

It is well-known that the performance of the cell is highly influenced by the oxygen reduction reaction (ORR) in cathode part, which needs a high overpotential to work [5]. This condition makes the cathode selection much more important in comparison to the anode choice. Elementary reactions in the cathode generally happened at the triple phase boundary (TPB) at electrode/electrolyte interface [6]. The TPB is defined as the site where the gas phase, the ion conductor and the electronic conductor of the oxygen are in contact with each other [7, 8]. To be considered as a good electrode material, the cathode must have strong electrochemical performance that can be measured by its electronic conductivity and

oxygen diffusivity; these properties are influenced by the ORR that occurs at the TBP cathode.

The cathode must be able to resist any chemical degradation that may occur during fuel cell operation and that can be determined making a comparison between the thermal expansion coefficient (TEC) and the stability of the electrode [9 – 11]. The mentioned characteristics not only depend on the interaction between the components forming the material but are also influenced by the size of the nanostructure and the composition of the cathode [12, 13]. New synthesis routes and unconventional compounds are the popular used strategies to propose new cathode materials and used as an alternative way to improve the performance of solid oxide fuel cells. Among the methodologies for the synthesis of new materials to the cathode, we find that doping the original composition with another element to produce a deformation within the structure is the most used since allows a better diffusivity of the oxygen ion. For example, strontium, calcium and barium, group II elements that have been used as dopants, according to the literature, can increase the conductivity of materials. Also, transition elements such as zinc, molybdenum or vanadium have also been reported as dopant agent to the cathode material, reporting interesting results from electrical measurements and polarization resistance [12].

The alteration of the structure in this type of materials to SOFC, has become one of the fields most studied since nanometric oxide materials have a higher catalytic performance due to present an increase in the surface vacancies, electronic and ionic conductivities [14]. Other synthesis methods as infiltration or impregnation, allows the construction of the nanostructure of the cathode material, by depositing the nanoparticles on a pre-sintered backbone (at high temperature), in that way, the electrocatalytic properties and stability of the cathode material are reached, while the costs of the synthesis can be reduced [14 – 16]. Cathode nanomaterials have generally been synthesized via solid-state reaction or sol-gel methods. However, since the cathode thickness influences the performance of SOFCs, other techniques such as inkjet printing, screen printing (SP), and electrophoretic deposition have been also proposed to fabricate more complex cathode structures [17, 18]. Parameters such as the temperature, time during annealing and sintering stage were also investigated to optimize the size of nanostructures, microstructural, magnetic and optical properties of different perovskite manganites [18, 19]. Additionally, a comparison of different synthesis methods has also been carried out to determine changes in electrical, microstructural and surface properties. For example, Da Conceição *et al.*, and coworkers

synthesized a lanthanum strontium manganite, $LSM=La_{0.7}Sr_{0.3}MnO_3$, using the combustion, sol-gel and a solid state reaction methods [20]. The authors found that all materials exhibited a single LSM phase formation with crystallite sizes in the range of 12 - 20 nm, whereas porosity, particle size and microstructure of the LSM sintered at high temperature are very dependent of the synthesis method. In this context, the samples synthesized by the combustion and sol-gel methods, compared to the other techniques, presented smaller particle sizes and higher porosity after the sintering process than that obtained from solid state synthesis; however, the electrical conductivity was found quite similar under the same composition [21].

The most popular cathode materials enclose perovskite nanostructures. This material is a mineral that contains the structure of calcium titanate ($CaTiO_3$), adopting the general formula of ABO_3. Thus, a wide variety of oxide compounds can have this type of structure and the properties can be modulated according to the final requirements. The orthorhombic structure is the most common among ABO_3 perovskite nanostructures. This type of structure includes many $LnMO_3$ compounds in which Ln is a trivalent rare earth combined with other transition metals and M is a trivalent cation (Al, Fe, Mn, Ga, Cr, V) [22]. As mentioned above, the doping strategy has been widely adopted to improve the performance of this kind of cathode materials for SOFCs applications [23]. Particularly, strontium-doped lanthanum manganite ($La_{1-x}Sr_xMnO_{3\pm d}$, LSM) also known as LSM is one of the earliest cathode materials that fill out a lot of the requirement for high-performance SOFCs. LSM nanostructures have good chemical and thermal stability, high catalytic activity in the reduction of the oxygen, and high electronic conductivity [24]; their thermal expansion coefficient similar to the solid electrolyte of yttria stabilized zirconia ($ZrO_2/Y_2O_3 - YSZ$) reduces the possibility of thermomechanical degradation due to the mismatch of length when the material is expanding while heating. Unfortunately, at low temperature, LSM nanostructures exhibits a very high polarization loss which inhibits its usage for IT-SOFC and LT-SOFC applications [25].

Among the nanostructured materials that can help to solve this problem during SOFCs operation, $LaMnO_3$ compounds have been proposed the. The lattice of these perovskites can be suitable to be doped with a combination of rare earths (RE), improving the compatibility at the cathode- electrolyte interphase and the kinetics of the oxygen reduction reaction. It is also known that the substitution of lanthanum by another ion directly modifies its characteristics due to

new interactions in the La-O and Mn-O bonds. Bhalla *et al.* present a review of this type of perovskites evaluating their role in ceramic science and technology, showing this structure is one of the most versatile in the area [26].

In this context, the partial substitution of La at the A-site by other rare earth ions has shown an improvement in overall cell performance by reducing cathode polarization, operating temperature and ionic-electrical resistivity, through RE-O and Mn-O interactions [27 – 30]. For example, electronic properties of Pr, Sm and Ce as part of the lanthanide series have similar properties compared to La, but can enhanced the electronic interaction in the final nanostructured compound favoring a specific property. The new interactions lead to a weak bond between the surface and adsorbed oxygen species provoking a low diffusion barrier for oxygen ions, thus facilitating the oxygen reduction reaction. [31, 32].

Continuing with the contribution of the research group of the Instituto Politécnico Nacional at UPII-Hidalgo in collaboration with Tecnológico Nacional de México- IT de Ciudad Madero and other research centers, in the development of nanostructured materials for energy production; at this opportunity, advances are reported in the synthesis of ABO$_3$-type perovskites nanostructures. It has been explored the La-substitution in the A-site of LaMnO$_3$ perovskites by different RE materials such as Ce, Sm, Pr to evaluate structural, morphological and electrical changes evaluating the alternative as cathode material for SOFCs. Specifically, this research reports the synthesis of rare earth cathode electrode nanomaterials, La$_{(1-x)}$Ln$_x$Ca$_{0.3}$MnO$_3$, by the Pechini method, using different stoichiometries in molar ratios (x=0.1, 0.3, 0.5 and 0.6; Ln=Ce, Sm, Pr). The crystal structure, morphological analysis and electrical measurements of the cathode materials were systematically investigated and discussed in terms of ORR activity.

2. Methodology

2.1. *Synthesis of perovskites nanoparticles*

Metal nitrates from Sigma Aldrich, were used as a precursors to the synthesis and consisted of lanthanum (III) nitrate hexahydrate (*La(NO$_3$)$_3$ * 6H$_2$O*, 99.99 % purity), praseodymium (III) nitrate hexahydrate (*Pr(NO$_3$)$_3$ * 6H$_2$O*, 99.9 % purity), samarium (III) nitrate hexahydrate (*Sm(NO$_3$)$_3$ * 6H$_2$O*, 99.9 % purity) calcium nitrate tetrahydrate (*Ca(NO$_3$)$_3$ * 4H$_2$O*, 99 % purity) and manganese (II) nitrate

tetrahydrate ($Mn(NO_3)_2 * 4H_2O$, 97.0 % purity). Stoichiometric amounts were calculated to obtain a nominal composition according to the chemical reaction to form $La_{0.7-x}Ln_xCa_{0.3}MnO_3$ (Ln=Sm, Pr, Ce; x=0.1, 0.3, 0.5 and 0.6) perovskites nanoparticles. The synthesis was performed as follows: first, the metal salts were placed in a matrass and mixed with the citric acid (CA) and deionized water, forming a 3:1 solution in relation to citric acid/metal cations. The solution was magnetically stirred for 10 min at 90 °C or 110 °C, respectively. Thereafter, ethylene glycol (EG) was added drop by drop (2 mL min^{-1}) up to reach a 2:1 ratio (EG/CA), maintaining the magnetic stirring for 4 or 5 h to obtain a gel. This gel was annealed at 450 °C for 3 h until the obtaining of powders which were grinded in an agate mortar. Finally, the samples were put through a heat treatment at 1000 °C for 6 h.

2.2. *Characterization*

The structural analysis of the as obtained nanoparticles was performed in an X-Ray diffractometer, Bruker D2 Phaser Lynx eye using a Bragg-Brentano (θ-2θ) configuration. Measurements were carried out with an applied voltage of 40 kV, current of 40 μA and a radiation Kα-Cu (λ=1.5406 Å). The scans were acquired in the θ-2θ range of 10° to 90°. The morphology of nanopowders was observed using a JEOL JSM-6701F microscope using 10 kV of accelerating voltage. Pellets were manufactured with the powders at 10 ton (1 cm²) to carry out the electrical tests. These measurements were carried out using four-point probe method at room temperature with a surface resistivity meter (SRM-232).

3. Results and discussion

It has been well recognized that depending on the applied temperature and the oxygen present in the lattice, this type of nanomaterials can crystallize in different symmetries, being the most common the cubic, orthorhombic and monoclinic [33]. Figure 1 shows the XRD patterns of the as-prepared $La_{0.7-x}Ln_xCa_{0.3}MnO_3$ (Ln=Sm, Pr, Ce; x=0.1, 0.3, 0.5 and 0.6) nanopowders.

It was observed that regardless of the Ln amount, the patterns display typical reflections of an orthorhombic perovskite-type structure (PDF #49-0416). But a displacement of the main reflections is observed as the content of the cations (Pr, Sm, Ce) increases. This behavior has been observed in other kind of perovskites and it is related to the expansion of the cell volume. It is also recognized

that impurities in the composition or interface can influence the stability performance of the SOFCs devices. In some compositions small peaks of a probable secondary phase formed during the synthesis process are observed. To estimate the size crystallites in the obtained perovskite, the Scherrer´s equation was used. Measurements were carried out based on the most representative signal of each sample (121). The as-obtain samples of praseodymium show a crystallite size (C.S.) between 61.2 and 73.5 nm, while in the case of samarium the samples show a variation between 64.3 and 71.5 nm; finally, for cerium, the C.S. was obtained in a range between 63.0 to 72.1 nm. The C.S. did not show a clear trend with the substitution of different cations, however the three substitutions coincide that the composition x=0.3, presented the minimum size in the samples: Pr^{3+} (61.2 nm), Sm^{3+} (64.3 nm) and Ce^{3+} (63.0 nm).

The contradiction with other previously reported lanthanum perovskites nanostructures, where a progressive increase in crystal size is observed with the amount of cationic dopant (30-49 nm), highlights the importance of both the size of the ionic radii as the amount of cation during La substitution to form ABO$_3$-type perovskites, as well as the synthesis process [34 – 36]. It is important to highlight that the XRD analyzes were carried out before applying the sintering process, however, the diffractograms did not show any representative signal corresponding to the typical perovskite structure, so it was concluded that a high applied temperature (1000 °C in this case) is necessary to achieve the formation of the desired ABO$_3$ structure.

Rietveld analysis is a method in which various parameters are adjusted to match XRD crystallographic data, being one of the best approaches to characterize nanocrystalline materials and extract information about the unit cell and quantitative amount of the phase. To confirm the formation of the secondary phase, Rietveld refinement was carried out using the FullProf Suite 64 software and a pseudo-Voigt function to compensate for stress or size contributions to signal broadening. The analysis was carried out from an orthorhombic system with a space group Pnma, determining the different parameters of the unit cell, the positions and atomic coordinates x and z for the corresponding elements. Table 1 shows the refinement parameters obtained for the different samples (Pr, Sm, Ce).

The results showed a variation in the occupancy of the site that was reflected in a correlation between the occupancy and the molar quantity of these elements. The results also showed that there is a reduction in the cell volume of the
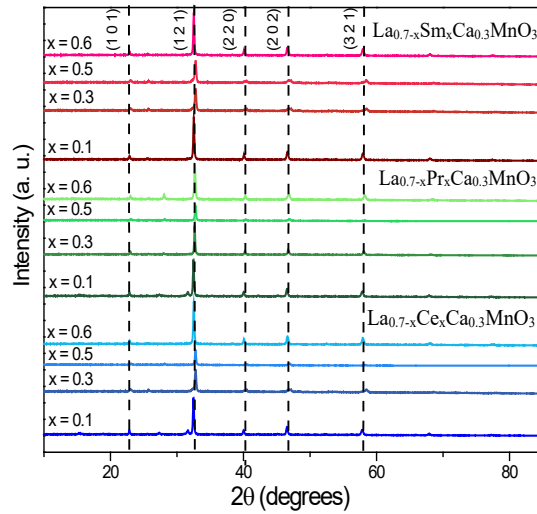
Figure 1. XRD patterns obtained for the $La_{(0.7-x)}Ln_xCa_{0.3}MnO_3$ (Ln = Sm, Pr, Ce; x=0.1, 0.3, 0.5 and 0.6) samples.

Table 1. Structural parameters obtained by Rietveld refinement

Sample	Composition	Phase	Cell Parameters			Volume	(χ^2)
			a ($\dot{A}$)	b ($\dot{A}$)	c ($\dot{A}$)	($\dot{A}^3$)	
Pr	0.1	Orthorhombic	5.433	7.667	5.467	227.76	3.48
	0.3		5.445	7.719	5.417	227.72	3.54
	0.5		5.428	7.666	5.476	227.92	4.03
	0.6		5.418	7.720	5.444	227.75	4.41
Sm	0.1	Orthorhombic	5.447	7.724	5.412	227.761	3.60
	0.3		5.450	7.723	5.404	227.518	4.28
	0.5		5.434	7.732	5.421	227.821	3.75
	0.6		5.445	7.735	5.409	227.849	5.31
Ce	0.1	Orthorhombic	5.678	7.722	5.601	245.57	5.718
	0.3		5.694	7.728	5.620	247.29	6.877
	0.5		5.512	7.731	5.419	235.181	4.92
	0.6		5.792	7.801	5.632	254.47	7.952

material by increasing the cation La cation substitution (x value) and therefore important differences in the lattice parameters depending on the composition. The increase of Pr, Sm or Ce in the synthesized nanocomposites causes an increase in the parameter a and a decrease in b and c, which confirms the existence

of distorted orthorhombic structures. From the obtained data, Vesta 3.5.7® software was used to represent the cell structure for each rare earth cation. Figure 2 a-c shows the cell for Pr, Sm and Ce at a composition of x=0.5, which were selected as representative.
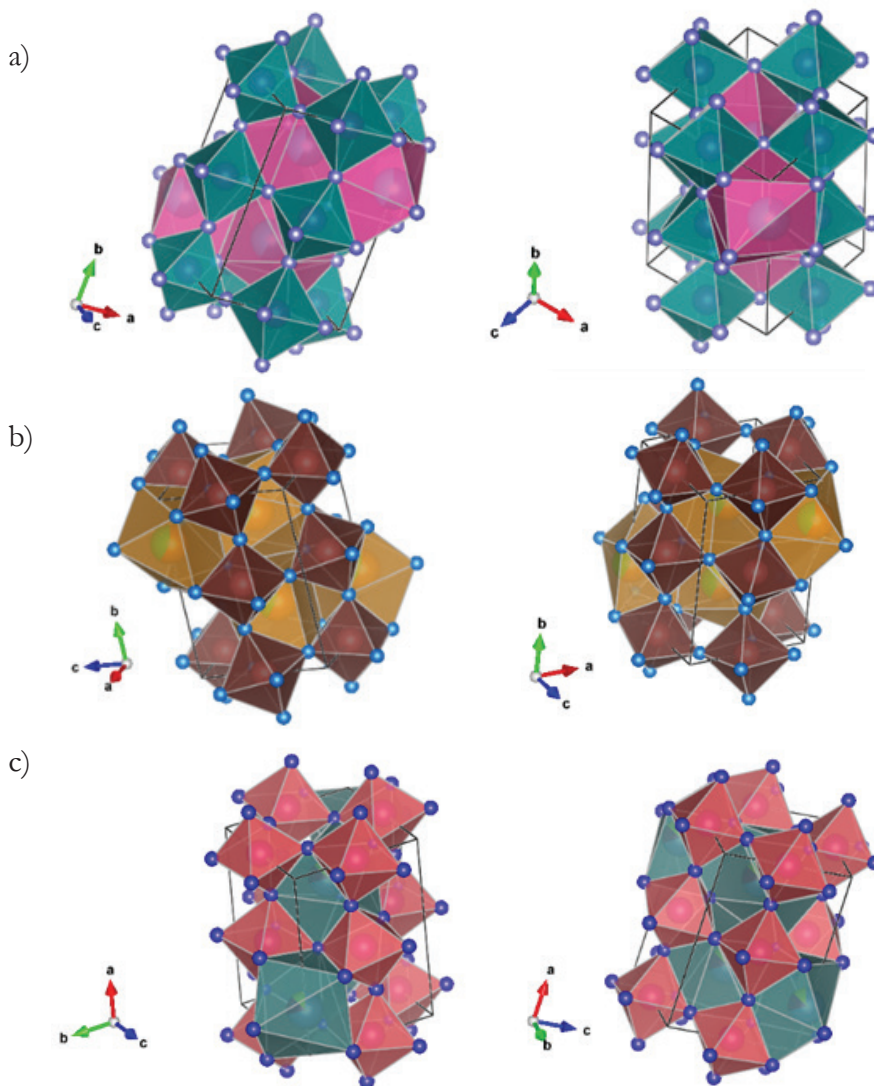

Figure 2. Unit cell drawn with the parameters obtained from Rietveld refinement:
a) praseodymium b) samarium c) cerium

It was determined that the unit cell of the synthesized materials is orthorhombic, regardless of the amount of cation (Pr, Sm, Ce) used, however, when analyzing the cell with the values obtained for parameters *a*, *b* and *c*, important

differences were observed in the direction of the distortion depending on the amount and ionic radii that replaced La. A similar trend was previously reported for strontium-doped perovskites, where refinement showed that the unit cell parameters a and c increased with increasing amount of Sr [37], while b parameter decreased, obtaining a distorted orthorhombic structure; which in turn correlated with the Jahn-Teller (JT) effect that modifies the Mn^{+3} ion into the octahedral Mn. JT can be understood as the geometric distortion of a nonlinear system reducing its symmetry and energy, which in turn influence ionic and electrical properties. Jahn Teller proposed that nonlinear degenerate molecules cannot be stable and that any highly symmetric molecule will undergo geometric distortion to reduce its symmetry and, thus, lower its energy.

From this Figure, the distances in the Mn-O bond for each nanomaterial were also analyzed, since this parameter indicated the distortion degree, and the results can be seen in Table 2. Considering that the order in the ionic radii in these rare earths are La(1.189 A)>Ce(1.155 A)>Sm(1.086 A)>Pr (1.069 A). In each distorted orthorhombic structure six Mn-O bonds were identified; each Mn-O bond in the structure was labeled as I and varies from 1 to 6. It is clear that the distortion in the materials is giving in different directions without clear tendency, with respect to lanthanum substitution.

Table 2. Distance of Mn – O bonds.

Bond	Distance Mn-O / Å											
	$La_{0.7-x}Pr_xCa_{0.3}MnO_3$				$La_{0.7-x}Sm_xCa_{0.3}MnO_3$				$La_{0.7-x}Ce_xCa_{0.3}MnO_3$			
	0.1	0.3	0.5	0.6	0.1	0.3	0.5	0.6	0.1	0.3	0.5	0.6
I1	1.968	1.964	1.968	1.968	1.962	1.966	1.962	1.966	1.999	1.996	1.999	1.997
I2	1.960	1.951	1.962	1.963	1.954	1.952	1.951	1.951	1.940	1.942	1.940	1.941
I3	1.968	1.964	1.968	1.968	1.962	1.966	1.962	1.966	1.999	1.996	1.999	1.997
I4	1.960	1.951	1.962	1.963	1.954	1.952	1.951	1.951	1.940	1.942	1.940	1.941
I5	1.957	1.969	1.957	1.956	1.970	1.967	1.972	1.971	1.971	1.968	1.970	1.968
I6	1.957	1.969	1.957	1.956	1.970	1.967	1.972	1.971	1.971	1.968	1.970	1.968
Angle (°)	Mn-Ox-Mn				Mn-Ox-Mn				Mn-Ox-Mn			
O1	157.57	157.45	157.58	157.44	157.46	157.47	157.42	157.45	159.21	159.32	159.22	159.31
O2	156.56	156.91	156.52	156.81	156.87	156.89	156.94	156.95	158.76	158.81	158.79	158.77

The JT effect was observed to occur in the prepared nanostructured perovskites along the bonds of Mn^{+3} cation. In $A-MnO_3$ manganites, the conducting electrons reside in the 3d Mn^{+3} orbitals. Due to its structure, the Mn ion is located

in the octahedral center and the 3d degenerate orbitals of Mn are strongly hybridized with the 2p orbitals of O [38, 39]; which can explain the irregular variations in the Mn-O bonds with respect to the composition.
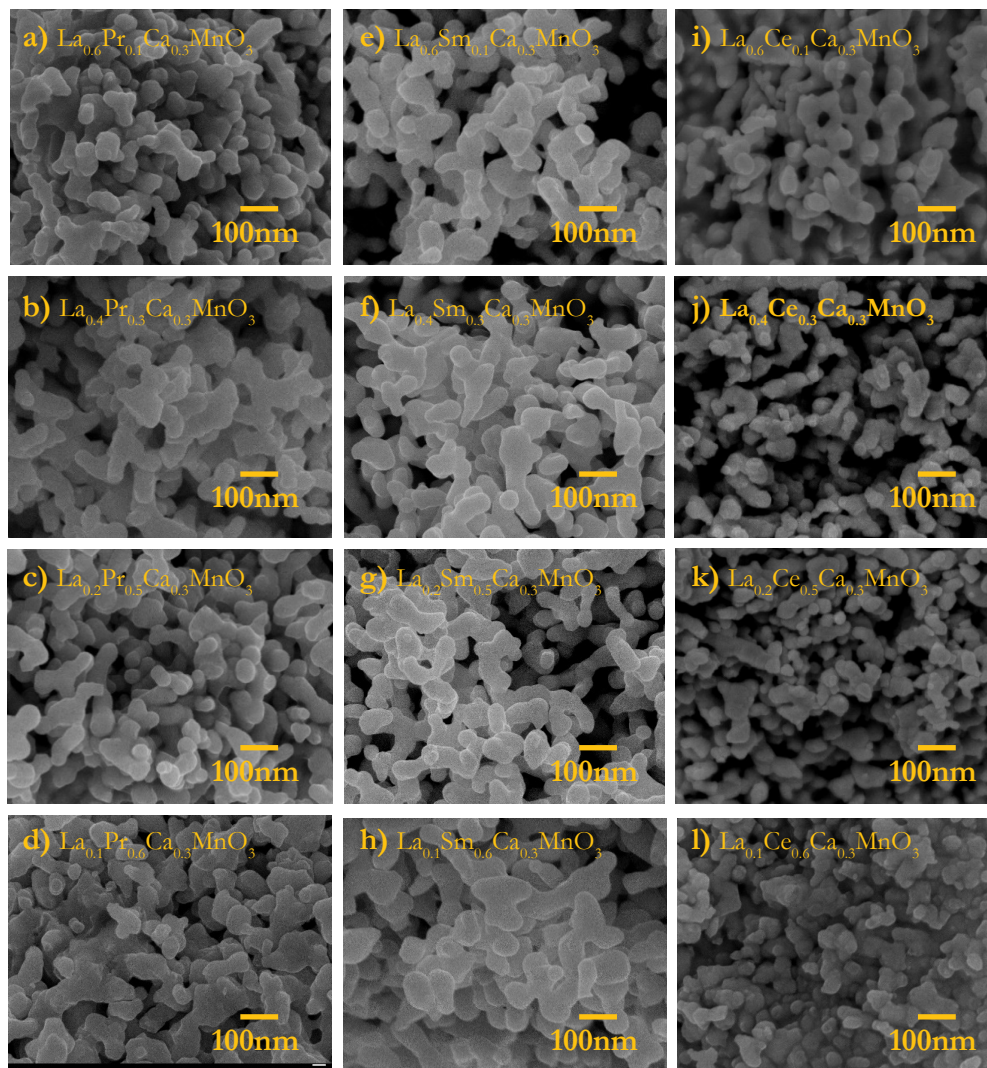

Figure 3. SEM observations for a-d) $La_{0.7-x}Pr_xCa_{0.3}MnO_3$, e-h) $La_{0.7-x}Sm_xCa_{0.3}MnO_3$ and, i-l) $La_{0.7-x}Ce_xCa_{0.3}MnO_3$ powders (x= 0.1, 0.3, 0.5, 0.6) after sintering process at 1000 °C.

The morphological analysis of the $La_{0.7-x}Pr_xCa_{0.3}$, $La_{0.7-x}Sm_xCa_{0.3}MnO_3$ and, $La_{0.7-x}Ce_xCa_{0.3}MnO_3$ powders sintered at 1000 °C can be seen in the Figure 2 a-l. From the micrographs, it is evident that that all samples present a granular structure, however a more compact morphology was obtained with the addition of

larger quantities of Pr, Sm or Ce ions. As a consequence, it can be observed that these assemblies present a less porous structure with well-connected agglomerate nanoparticles in the submicron size, which conditioned the gas diffusion towards the triple point boundary. Different materials with a similar microstructure have been reported indicating that they may be a suitable material for SOFC cathode at intermediate temperatures.

The electrical performance was analyzed using four-point probe, which is a common technique for evaluating the resistivity value of a layer in conductive nanomaterials that can be used in electrical devices. Then, measurements were carried out on green and sintered pellets (1 cm in diameter, 1000 °C, 4 h). Table 3 shows the parameters obtained to analyze the electrical performance in the pero-vskite-type nanostructures depending on the composition and ion substitution, as well as the potential application in SOFCs.

Table 3. Results obtained by the four-point probe.

Perovskite		Resistance (Ω sq^{-1})	Resistivity (Ω cm)	Conductivity (10^{-4} S cm^{-1})
$La_{0.7-x}Pr_xCa_{0.3}MnO_3$	0.1	36.6	4.76	2100.8
	0.3	35.5	4.54	2158.9
	0.5	79.7	10.30	970.8
	0.6	78.2	9.81	977.9
$La_{0.7-x}Sm_xCa_{0.3}MnO_3$	0.1	64	9.83	1017.1
	0.3	22.9	3.56	2803.3
	0.5	18.5	4.84	2064.3
	0.6	35.2	9.19	1087.5
$La_{0.7-x}Ce_xCa_{0.3}MnO_3$	0.1	28.8	3.80	2630.4
	0.3	26.4	3.46	2884.7
	0.5	---	---	---
	0.6	15.1	1.97	5070.2

The obtained values of conductivity for the praseodymium nanostructures are observed between 0.09 to 0.21 Scm^{-1}. For the Samarium samples, values from 0.10 to 0.28 Scm^{-1} were obtained. To the Cerium, the results present conducti-vity in a range of 0.26 to 0.5 Scm^{-1}. In general, the highest conductivity in the case of La substitution in the nanocomposites was observed with Pr and Sm at a composition of x = 0.3, showing a decrease in the values when the amount of the cation is higher. On the contrary, the behavior observed for Ce substituted

lanthanum, presents a tendency related to the doping applied, with the highest value reported at x=0.6 (0.5 Scm^{-1}). Previously, it has been found that in lanthanum-strontium-manganese (LSM) perovskites, the incorporation of Sr^{+2} in the ABO$_3$-type structure favors conductivity in relation to the amount of doping used, obtaining values in intervals greater than 200 Scm^{-1} with temperatures between 600-900 °C [39]. This behavior occurs at the expense of an increase in the content of Mn^{4+} in the final structure. Then, considering that measurements have been realized at room temperature and an important increased with the operating temperature of SOFCs is expected, the synthesized nanomaterials can be an alternative for scalable applications.

4. Conclusions

In this work, the synthesis of ABO$_3$-type perovskites has been analyzed, particularly LaMnO$_3$ nanoparticles by doping the A-site with other rare earth, as an efficient alternative cathode material for SOFCs. Then, this research reports the synthesis of rare earth cathode electrode materials, $La_{(1-x)}Ln_xCa_{0.3}MnO_3$, by the Pechini method, using different stoichiometries in molar ratios (x=0.1, 0.3, 0.5 and 0.6; Ln=Ce, Sm, Pr). From the above results the following results can be mentioned:

According to the crystallographic chart PDF490416, the observed signals are the characteristics of nanomaterials with an orthorhombic phase. XRD analyzes were performed before applying the heat treatment; however, the spectra did not show any representative signal of the sample, so it is concluded that the applied temperature is what leads to the formation of the desired nanostructured perovskite. From the results obtained through the Scherrer's equation for the crystallite size, it was observed that they present average values greater than 50 nm, but according to the consulted literature, they are within the reported interval.

After the Rietveld analysis, information was obtained on the unit cell of the perovskite type nanomaterial, the results represented a variation in the site occupation factor that was reflected in a correlation between the occupation and the molar quantity of these elements. It was determined that the unit cell of the synthesized nanomaterials is orthorhombic, regardless of the amount of cation (Pr, Sm, Ce) used and presenting a pure phase. The drawing of the cell with the values obtained for the lattice parameters *a*, *b*, *c* shows a distortion and cell

volume that depends on the ionic radii as well as the amount of the rare cation that replaces La. The observed micrographs show that the growth of the nanostructures is similar even when their stoichiometric ratio changes, being almost entirely homogeneous.

The values obtained by the four-point probe method did not show a clear trend; however, it is possible to appreciate that Sm (2803.3 x 10-4 S cm^{-1}) and Pr (2158.9 x 10-4 S cm^{-1}) at x=0.3 and displayed high conductivities whereas the highest electrical properties for Ce is observed at x=0.6. Test at high temperatures to evaluate coefficient of thermal expansion and electrochemical performance are ongoing to confirm this trend.

Acknowledgement

Funding

References

1. Selmi, T., Khadhraoui, A., & Cherif, A. (2022). Fuel cell–based electric vehicles technologies and challenges. *Environmental Science and Pollution Research*, 29, 78121-78131.
    https://doi.org/10.1007/s11356-022-23171-w

2. Fan, L., Tu, Z., & Chan, S. H. (2021). Recent development of hydrogen and fuel cell technologies: A review. *Energy Reports*, 7, 8421-8446.
    https://doi.org/10.1016/j.egyr.2021.08.003

3. Raza, T., Yang, J., Wang, R., Xia, C., Raza, R., Zhu, B. *et al.* (2022). Recent advance in physical description and material development for single component SOFC: A mini-review. *Chemical Engineering Journal*, 444, 136533.
    https://doi.org/10.1016/j.cej.2022.136533

4. Ahmad, M. Z., Ahmad, S. H., Chen, R. S., Ismail, A. F., Hazan, R. *et al.* (2022). Review on recent advancement in cathode material for lower and intermediate temperature solid oxide fuel cells application. *International Journal of Hydrogen Energy*, 47(2), 1103-1120.
    https://doi.org/10.1016/j.ijhydene.2021.10.094

5. Hauch, A., Küngas, R., Blennow, P., Hansen, A. B., Hansen, J. B., Mathiesen, B. V. *et al.* (2020) Recent advances in solid oxide cell technology for electrolysis. *Science*, 370(6513), aba6118.
    https://doi.org/10.1126/science.aba6118

6. Wang, M., & Feng, Z. (2021). Interfacial processes in electrochemical energy systems. *Chemical Communications*, 57, 10453-10468.
    https://doi.org/10.1039/D1CC01703A

7. Papac, M., Stevanović, V., Zakutayev, A., & Hayre, R. O'. (2020). Triple ionic–electronic conducting oxides for next-generation electrochemical devices. *Nature Materials*, 20, 301-313.
    https://doi.org/10.1038/s41563-020-00854-8

8. Sun, C., Alonso, J. A., & Bian, J. (2021). Recent Advances in Perovskite-Type Oxides for Energy Conversion and Storage Applications. *Advanced Energy Materials*, 11(2), 2000459.
    https://doi.org/10.1002/aenm.202000459

9. Abd Aziz, A. J., Baharuddin, N. A., Somalu, M. R., & Muchtar, A. (2020). Review of composite cathodes for intermediate-temperature solid oxide fuel cell applications. *Ceramics International*, 46(15), 23314-23325.
    https://doi.org/10.1016/j.ceramint.2020.06.176

10. Afroze, S., Reza, Md. S., Amin, M. R., Taweekun, J., & Azad, A. (2022). Progress in nanomaterials fabrication and their prospects in artificial intelligence towards solid oxide fuel cells: A review. *International Journal of Hydrogen Energy*.
    https://doi.org/10.1016/j.ijhydene.2022.11.335

11. Singh, M., Zappa, D., & Comini, E. (2021). Solid oxide fuel cell: Decade of progress, future perspectives and challenges. *International Journal of Hydrogen Energy*, 46(54), 27643-27674.
https://doi.org/10.1016/j.ijhydene.2021.06.020

12. Gunkel, F., Christensen, D. V., Chen, Y. Z., & Pryds, N. (2020). Oxygen vacancies: The (in)visible friend of oxide electronics. *Applied Physics Letters*, 116, 120505.
https://doi.org/10.1063/1.5143309

13. Zarabi Golkhatmi, S., Asghar, M. I., & Lund, P. D. (2022). A review on solid oxide fuel cell durability: Latest progress, mechanisms, and study tools. *Renewable and Sustainable Energy Reviews*, 161, 112339.
https://doi.org/10.1016/j.rser.2022.112339

14. Tarancón, A., Burriel, M., Santiso, J., Skinner, S. J., & Kilner, J. A. (2010). Advances in layered oxide cathodes for intermediate temperature solid oxide fuel cells. *Journal of Materials Chemistry*, 19, 3799-3813.
https://doi.org/10.1039/b922430k

15. Sreedhar, I., Agarwal, B., Goyal, P., & Agarwal, A. (2020). An overview of degradation in solid oxide fuel cells-potential clean power sources. *Journal of Solid State Electrochemistry*, 24, 1239-1270.
https://doi.org/10.1007/s10008-020-04584-4

16. Ko, H. J., Myung, J.-h., Hyun, S.-H., & Chung, J. S. (2012). Synthesis of LSM–YSZ–GDC dual composite SOFC cathodes for high-performance power-generation systems. *Journal of Applied Electrochemistry*, 42, 209-215.
https://doi.org/10.1007/s10008-020-04584-4

17. Rashidian Vaziri, M. R., Hajiesmaeilbaigi, F., & Maleki, M. H. (2011). Monte Carlo simulation of the subsurface growth mode during pulsed laser deposition. *Journal of Applied Physics*, 110, 043304.
https://doi.org/10.1063/1.3624768

18. Xia, W., Wu, H., Xue, P., & Zhu, X. (2018). Microstructural, Magnetic, and Optical Properties of Pr-Doped Perovskite Manganite $La_{0.67}Ca_{0.33}MnO_3$ Nanoparticles Synthesized via Sol-Gel Process. *Nanoscale Research Letters*, 13, 135.
https://doi.org/10.1186/s11671-018-2553-y

19. Baharuddin, N. A., Muchtar, A., Somalu, M. R., Anwar, M., Hameed, M. A. S. A. K. A., & Mah, J. (2017). Effects of sintering temperature on the structural and electrochemical properties of $SrFe_{0.5}Ti_{0.5}O_{3-\delta}$ perovskite cathode. *International Journal of Applied Ceramic Technology*, 15(2), 338-348.
https://doi.org/10.1111/ijac.12825

20. da Conceição, L., Silva, C. R. B., Ribeiro, N. F. P., & Souza, M. M. V. M. (2009). Influence of the synthesis method on the porosity, microstructure and electrical properties of La$_{0.7}$Sr$_{0.3}$MnO$_3$ cathode materials. *Materials Characterization*, 60(12), 1417-1423.
https://doi.org/10.1016/j.matchar.2009.06.017

21. Vismaya, J., Vinaya, J., Clementz Edwardraj, F. C., & Arputharaj S. N. (2022). Spinel-based electrode materials for application in electrochemical supercapacitors – present status and future prospects. *Inorganic and Nano-Metal Chemistry*, 52, 1449-1462.
https://doi.org/10.1080/24701556.2021.1956968

22. Hwang, L., Heuer, A. H., & Mitchell, T. E. (1973). On the space group of MgAl$_2$O$_4$ spinel. *Philosophical Magazine*, 28, 241-243.
https://doi.org/10.1080/14786437308217448

23. Zhang, Y., Yang, G., Chen, G., Ran, R., Zhou, W., & Shao, Z. (2016). Evaluation of the CO$_2$ Poisoning Effect on a Highly Active Cathode SrSc$_{0.175}$Nb$_{0.025}$Co$_{0.8}$O$_{3-\delta}$ in the Oxygen Reduction Reaction. *ACS Applied Materials & Interfaces*, 8(5), 3003-3011.
https://doi.org/10.1021/acsami.5b09780

24. Jain, U., Soni, S., & Chauhan, N. (2022). Application of perovskites in bioimaging: the state-of-the-art and future developments. *Expert Review of Molecular Diagnostics*, 22(9), 867-880.
https://doi.org/10.1080/14737159.2022.2135990

25. Ko, M.-H., Yoo, Y.-S., & Hwang, J.-H. (2015). Electrochemical estimation of GB-CO(GdBaCo2O5+δ)/GDC(Gd$_2$O$_3$-doped CeO$_2$) cathode composites designed for intermediate-temperature solid oxide electrochemical cells. *Ceramics International*, 41(3), 4616-4620.
https://doi.org/10.1016/j.ceramint.2014.12.005

26. Bhalla, A. S., Guo, R., & Roy, R. (2000). The Perovskite Structure – A Review of Its Role in Ceramic Science and Technology. *Material Research Innovations*, 4(1), 3-26.
https://doi.org/10.1007/s100190000062

27. Frozandeh-Mehr, E., Malekzadeh, A., Ghiasi, M., Gholizadeh, A., Mortazavi, Y., & Khodadadi, A. (2012). Effect of partial substitution of lanthanum by strontium or bismuth on structural features of the lanthanum manganite nanoparticles as a catalyst for carbon monoxide oxidation. *Catalysis Communications*, 28, 32-37.
https://doi.org/10.1016/j.catcom.2012.08.009

28. Solanki, S., Dhruv, D., Boricha, H., Zankat, A., Rathod, K. N., Rajyaguru, B. *et al.* (2020). Charge transport mechanisms and magnetoresistance behavior of La$_{0.6}$Pr$_{0.1}$Ca$_{0.3}$MnO$_3$ manganite. *Journal of Solid State Chemistry*, 288, 121446.
https://doi.org/10.1016/j.jssc.2020.121446

29. Ferrel-Alvarez, A. C., Domínguez-Crespo, M. A., Cong, H., Torres-Huerta, A. M., Palma-Ramírez, D., & Irvine, J. T. S. (2021). Microwave irradiation synthesis to obtain La0.7-xPrxCa0.3MnO3 perovskites: Electrical and electrochemical performance. *Journal of Alloys and Compounds*, 851, 156882.
https://doi.org/10.1016/j.jssc.2020.121446

30. Chourasia, R., & Shrivastava, O. P. (2012). Crystal structure and impedance study of samarium substituted perovskite: $La_{1-x}Sm_xMnO_3$ (x=0.1-0.3). *Solid State Sciences*, 14(3), 341-348.
https://doi.org/10.1016/j.solidstatesciences.2011.12.007

31. Gu, Q., Wang, L., Wang, Y., & Li, X. (2019). Effect of praseodymium substitution on $La_{1-x}Pr_xMnO_3$ (x=0–0.4) perovskites and catalytic activity for NO oxidation. *Journal of Physics and Chemistry of Solids*, 133, 52-58.
https://doi.org/10.1016/j.solidstatesciences.2011.12.007

32. Li, W., Xiong, C. Y., Jia, L. C., Pu, J., Chi, B., Chen, X. *et al.* (2015). Strontium-doped samarium manganite as cathode materials for oxygen reduction reaction in solid oxide fuel cells. *Journal of Power Sources*, 284, 272-278.
https://doi.org/10.1016/j.solidstatesciences.2011.12.007

33. Hammond, C. (2015). Chapter 4. Crystal symmetry: point groups, space groups, symmetry-related properties and quasiperiodic crystals. In: C. Hammond (Ed.). The Basics of Crystallography and Diffraction. *Oxford University Press*.
https://doi.org/10.1093/acprof:oso/9780198738671.003.0004

34. Ostroushko, A. A., Russkikh, O. V., & Maksimchuk, T. Y. (2021). Charge generation during the synthesis of doped lanthanum manganites via combustion of organo-inorganic precursors. *Ceramics International*, 47(15), 21905-21914.
https://doi.org/10.1093/acprof:oso/9780198738671.003.0004

35. Dinamarca, R., Sepúlveda, C., Delgado, E. J., Peña, O., Fierro, J. L. G., & Pecchi, G. (2016). Electronic properties and catalytic performance for DME combustion of lanthanum manganites with partial B-site substitution. *Journal of Catalysis*, 338, 47-55.
https://doi.org/10.1016/j.jcat.2016.02.011

36. Yue, C., Zhang, W., Wang, M., Liu, J., Zhang, J., & Hou, D. (2022). Crystal structure and octahedral deformation of orthorhombic perovskite ABO_3: Case study of $SrRuO_3$. *Journal of Solid State Chemistry*, 309, 122998.
https://doi.org/10.1016/j.jssc.2022.122998

37. Nagaraja, B. S., Rao, A., Babu, P. D., & Okram, G. S. (2015). Structural, electrical, magnetic and thermal properties of $Gd_{1-x}Sr_xMnO_3$ (0.2≤x≤0.5) manganites. *Physica B: Condensed Matter*, 479, 10-20.
https://doi.org/10.1016/j.jssc.2022.122998

38. Kamboj, V., & Ranjan, C. (2022). Chapter 11. Oxygen reduction reaction in solid oxide fuel cells. In: K. Sengupta, S. Chatterjee, K. Dutta (Eds.) *Oxygen Reduction Reaction*. Elsevier, pp. 379-426.
https://doi.org/10.1016/j.jssc.2022.122998

39. Moriche, R., Marrero-López, D., Gotor, F. J., & Sayagués, M. J. (2014). Chemical and electrical properties of LSM cathodes prepared by mechanosynthesis. *Journal of Power Sources*, 252, 43-50.
https://doi.org/10.1016/j.jpowsour.2013.11.093